Scripta Materialia 168 (2019) 76–80

Contents lists available at ScienceDirect

Scripta Materialia

journal homepage: www.elsevier.com/locate/scriptamat

Influences of hydrogen charging method on the hydrogen distribution and nanomechanical properties of face-centered cubic high-entropy alloy: A comparative study

Yakai Zhao [a], Jeong-Min Park [b], Dong-Hyun Lee [c], Eun Ju Song [d], Jin-Yoo Suh [e,*], Upadrasta Ramamurty [f,*,1], Jae-il Jang [b,*]

[a] School of Materials Science and Engineering, Beijing Institute of Technology, Beijing 100081, China
[b] Division of Materials Science and Engineering, Hanyang University, Seoul 04763, Republic of Korea
[c] Max-Planck-Institut für Eisenforschung GmbH, Max-Planck-Straße 1, Düsseldorf 40237, Germany
[d] Sandia National Laboratories, Livermore, CA 94550, USA
[e] High Temperature Energy Materials Research Center, Korea Institute of Science and Technology, Seoul 02792, Republic of Korea
[f] School of Mechanical and Aerospace Engineering, Nanyang Technological University, Singapore 639798, Singapore

ARTICLE INFO

Article history:
Received 4 April 2019
Accepted 22 April 2019
Available online 30 April 2019

Keywords:
High-entropy alloy
Hydrogen charging method
Hydrogen distribution
Nanoindentation
Thermal desorption spectroscopy

ABSTRACT

The influence of charging method on hydrogen (H) distribution and the resultant nanomechanical behavior of CoCrFeMnNi high-entropy alloy was examined and compared with another face-centered cubic structured alloy, an austenitic stainless steel. Through thermal desorption spectroscopy measurement and theoretical analysis, it was revealed that electrochemical (E-) charging induces steep gradient of H concentration near the surface while H was homogenously distributed after gaseous (G-) charging. Nanoindentation results show significant hardening in E-charged alloys while the hardness of G-charged alloys remains invariant. These differences were rationalized in terms of the nature of H distributions induced by different charging methods.

The emerging concept of high-entropy alloy (HEA) has significantly increased alloy design space [1–4]. In addition to outstanding cryogenic properties [5], exceptional strengthening effect [6,7], and good resistances to creep [8] and corrosion [9,10], it was found that HEAs are also highly resistant to hydrogen (H) embrittlement [11–15]. A crucial aspect, which is often overlooked not only for HEAs but also for most metallic materials in laboratory scale studies, is how the method employed for charging H affects the measured response. This paper focuses on this aspect.

In general, charging of H into a material is conducted through either gaseous or electrochemical charging (hereafter, referred to as G- and E-charging, respectively) [16–18]. The former is performed in a highly pressurized H_2 gas environment and at an elevated temperature [19], while the latter is conducted in an electrolytic solution under either galvanostatic or potentiostatic condition at or near room temperature (RT) [16]. Table 1 summarizes the literature data on H charging condition and resultant H content in HEAs [11–14,20–25]. It is obvious that both charging methods have been widely used and the resultant H contents vary considerably. These variations often lead researchers to markedly different conclusions. For example, in CoCrFeMnNi HEA, through E-charging, Luo et al. [12] reported a mild increase in plasticity while Zhao et al. [24] found significant hardening; through G-charging, Zhao et al. [11] reported no ductility loss whereas Nygren et al. [21] observed H embrittlement. The discrepancies may be attributed to the different charging methods and conditions employed in these studies, since they can lead to various H contents and trapping states. To shed light on this, we performed nanoindentation and thermal desorption spectroscopy (TDS) experiments on G- and E-charged CoCrFeMnNi HEA, which is one of the mostly investigated HEAs to date and was also widely selected for H-related studies as shown in Table 1. The results were compared with those of an austenitic stainless steel, 316L, since they both share the same face-centered cubic (FCC) structure and similar main constituent elements (only differ in relative content) [5,11].

Samples of the equiatomic CoCrFeMnNi HEA were prepared by vacuum induction casting, followed by hot-forging and solution annealing (1100 °C, 1 h) so as to obtain an alloy with a single FCC phase structure that has homogeneous composition [24]. For comparison purpose,

* Corresponding authors.
E-mail addresses: jinyoo@kist.re.kr (J.-Y. Suh), uram@ntu.edu.sg (U. Ramamurty), jijang@hanyang.ac.kr (J. Jang).
[1] Professor Upadrasta Ramamurty was an editor of the journal during the review period of the article. To avoid a conflict of interest, Prof. Jeff Th. M. DeHosson acted as editor for this manuscript.

https://doi.org/10.1016/j.scriptamat.2019.04.025
1359-6462/

Table 1
Comparison of H charging condition and resultant H content in various HEAs from literature. Note that the electrolytic solution used for E-charging is another important factor affecting H content but is not listed here. Detailed information can be found in each reference.

Composition	H charging condition					H content [wppm]	Ref.
	Charging method	H_2 pressure [MPa]	Current density [mA/cm^2]	Time [h]	Temperature [°C]		
CoCrFeMnNi	G-charging	15	–	72	300	63.2	[14]
		15	–	72	300	76.5	[11]
		100	–	200	300	113	[20]
		120	–	160	200	146.9	[21]
CoCrFeNi		120	–	160	200	58.5	[22]
$Fe_{50}Mn_{30}Cr_{10}Co_{10}$		100	–	200	300	113	[20]
CoCrFeMnNi	E-charging	–	1	48	RT	2.79	[23]
		–	7	48	RT	3.69	
		–	1	21	67	4.87	
		–	1	24	67	5.41	
		–	1	24	87	7.83	
		–	20	18	RT	7.73	[13]
		–	15	12	RT	8.01	[12]
		–	25	72	RT	15.22	
		–	100	240	RT	33.25	
		–	100	24	RT	45	[24]
$Co_{19.9}C_{r19.9}Fe_{19.9}Mn_{19.9}Ni_{19.9}C_{0.5}$		–	20	24	RT	5.65	[25]

solution-annealed 316L (nominal composition (in wt%): Fe-16.5Cr-9.77Ni-1.29Mn-0.19Co-2.07Mo-0.27Cu-0.5Si-0.02C) samples were also prepared. All the specimens were initially ground with fine SiC papers (grit number up to 2000) and then polished with colloidal silica (0.05 μm) to a mirror finish. The final thickness of each polished specimen is ~300 μm.

A custom-made Sieverts apparatus was utilized for G-charging of H_2 at 300 °C under constant pressure of 15 MPa for 72 h. A potentiostat/galvanostat equipment (HA-151A, Hokuto Denko, Tokyo, Japan) was utilize for E-charging in 1 N H_2SO_4 solution for 24 h at RT and under a constant current density of 100 mA/cm^2. Upon the completion of charging, all the charged samples were immediately immersed into liquid nitrogen and stored until further experiments to minimize possible H outgassing; in any case, subsequent experiments were performed within ~24 h after charging.

Nanoindentation experiments were conducted using the Nanoindenter-XP (formerly MTS; now KLA-Tencor, Milpitas, CA, USA) equipped with Berkovich tip. A peak load, P_{max}, of 100 mN and constant indentation strain rate of 0.025 s^{-1} [26] were employed. For the quantitative analysis of the H content in the charged samples, TDS analysis was conducted with a quadrupole mass spectroscope (EX0014, R-DEC Company, Tsukuba, Japan) at a constant heating rate of 5 °C/min.

Representative nanoindentation load–displacement (*P*-*h*) responses obtained on both HEA and 316L samples are provided in Fig. 1a. Variations in the hardness values of the uncharged and H charged specimens, extracted from the *P*-*h* curves using the Oliver-Pharr method [27], are displayed in Fig. 1b. While E-charging significantly hardens (by ~63%) both HEA and 316L, only a marginal hardening is noted upon G-charging. The ratio of the final displacement after unloading, h_f, to the maximum displacement, h_{max}, is proportional to W_p/W_{tot} where W_p is the irreversible, plastic work of indentation (i.e., the area enclosed by loading and unloading curve) and W_{tot} is the total work of indentation (i.e., the area under the loading curve) [28]. Hence, h_f/h_{max} is a useful indicator of the relative portion of the plastic deformation in the total elasto-plastic deformation that occurs during indentation. Note that, in the present work, h_f was determined by fitting the early 90% portion of unloading curve (shown unloading part in Fig. 1a) following P vs. h^2 fit so as to avoid slight h change that occurs during thermal drift correction process at $0.1P_{max}$. Estimated values of h_f/h_{max} are displayed in Fig. 1c. While the ratios of G-charged HEA and 316L samples are similar to the respective uncharged ones, h_f/h_{max} of E-charged samples are significantly lower, indicating an increased tendency of H embrittlement due to E charging.

TDS measurements were employed to gain insights into the reasons for the observed differences in the hardening behavior of E- and G-charged specimens. Fig. 2a displays the thermal desorption profiles obtained. Two features are noteworthy. First, for the same charging process, HEA always shows a much higher H content than 316L, which is in a good agreement with prior reports of higher H solubility in CoCrFeMnNi HEA than in other FCC alloys [11,21]. The higher H solubility in the HEA has been attributed to the relatively high Cr and Mn contents, which are known to enhance H solubility [11,19], the high lattice strain energy in HEA [3,14], and a possible contribution from short-range order [14,29]. The second observation from Fig. 2a is that, the two different charging processes employed lead to different desorption behavior. While the main desorption peaks of both E-charged specimens appear at ~135 °C, those of G-charged ones occur at significantly higher temperatures (~300–330 °C). In TDS, heating causes "detrapping" of H first and then diffusion of it through the lattice so as to escape from the surface. Hence, the differences in the desorption spectra of G- and E-charged specimens can be due to either H detrapping from different trapping sites or different resistances for H diffusion. In FCC metals and alloys, H diffusion is slower than the detrapping process, and thus the rate-controlling stage for the thermal desorption process during TDS is H diffusion rather than H detrapping [30]. This means that the difference in the peak temperatures is more likely to be related with difference in average H diffusion distance within G- and E-charged specimens. Indeed, E-charging at RT was reported to create a high surface concentration of H in conventional alloys [17,18], which would surely lead to a shorter diffusion path for the majority of H atoms compared to the case of homogeneous H distribution.

For a more direct confirmation of such an inhomogeneous H distribution in E-charged FCC alloys, additional TDS measurements were performed. Immediately after E-charging, the charged side of the CoCrFeMnNi sample was ground such that only half of the sample remains (as schematically illustrated in the inset of Fig. 2b). The TDS spectrum obtained from it is compared with that of "unground" sample in Fig. 2b. The H concentration in half sample is ~1.9 weight ppm (hereinafter "wppm"), which is only marginally larger than that measured in the uncharged sample (~1.7 wppm). This observation implies that almost all the charged H is near/closer to the surface of the sample that was charged. In contrast, TDS measurements conducted on back half samples of an E-charged ferritic steel with body-centered cubic (BCC) matrix [18] show that ~32% of total H amount resides in the back half sample. This implies that although a H concentration gradient also exists in the E-charged ferritic steel sample, the gradient is much less steep as compared to the current case of FCC HEA. This observation points to one of the key differences in H behavior between FCC and BCC metals: the diffusivity of H in the latter is much higher—generally 4 to 5 orders of magnitude at RT—than in the former [31]. In contrast, the solubility of

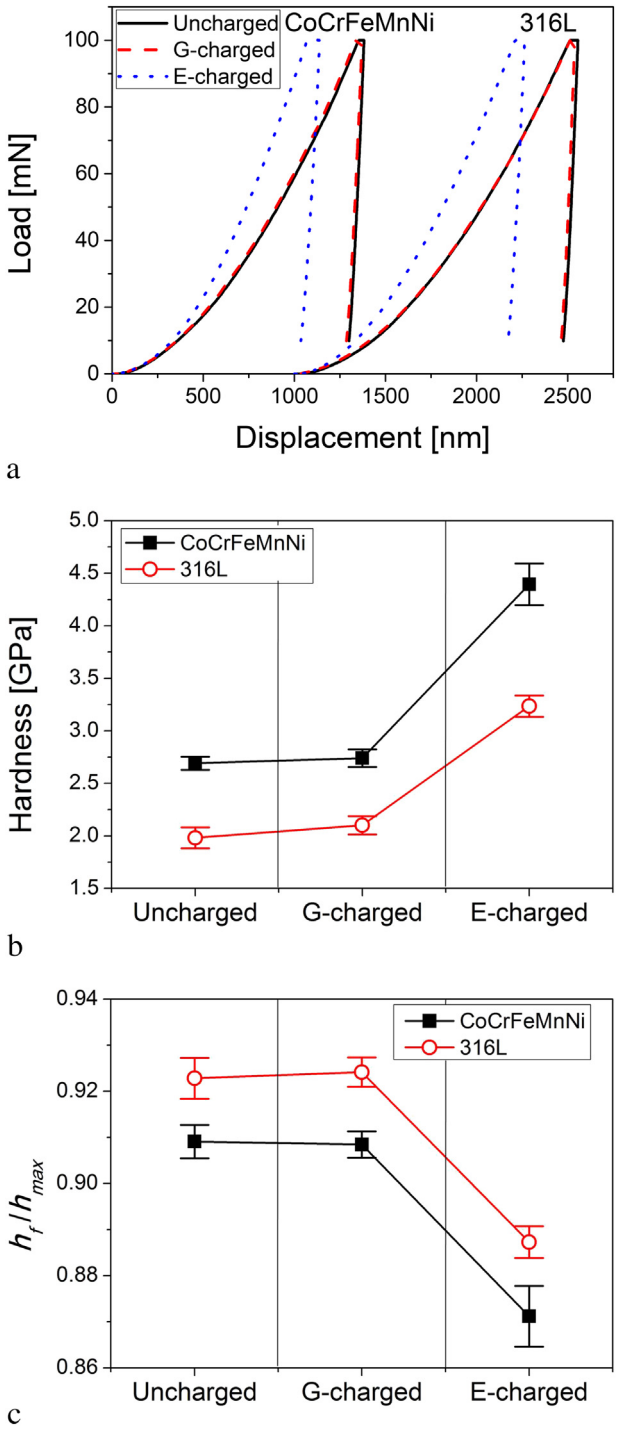

Fig. 1. Nanoindentation results: (a) representative load-displacement (*P-h*) curves, (b) variations in nanoindentation hardness, and (c) variations in the ratio of the final displacement (h_f) to maximum displacement (h_{max}) of CoCrFeMnNi HEA and 316L austenitic stainless steel in uncharged, G-charged and E-charged states.

H is much higher in FCC metals. The combination of these factors lead to a large concentration gradient in the E-charged FCC alloys, including the CoCrFeMnNi HEA and 316L steel investigated in the present work.

A first order approximation of the H concentration gradient in E-charged samples can be made as following. The local H content as a function of the distance from the surface, *x*, can be estimated as [32]:

$$C(x,t_c) = C_0\left[1 - erf\left(\frac{x}{2\sqrt{D_H t_c}}\right)\right], \quad (1)$$

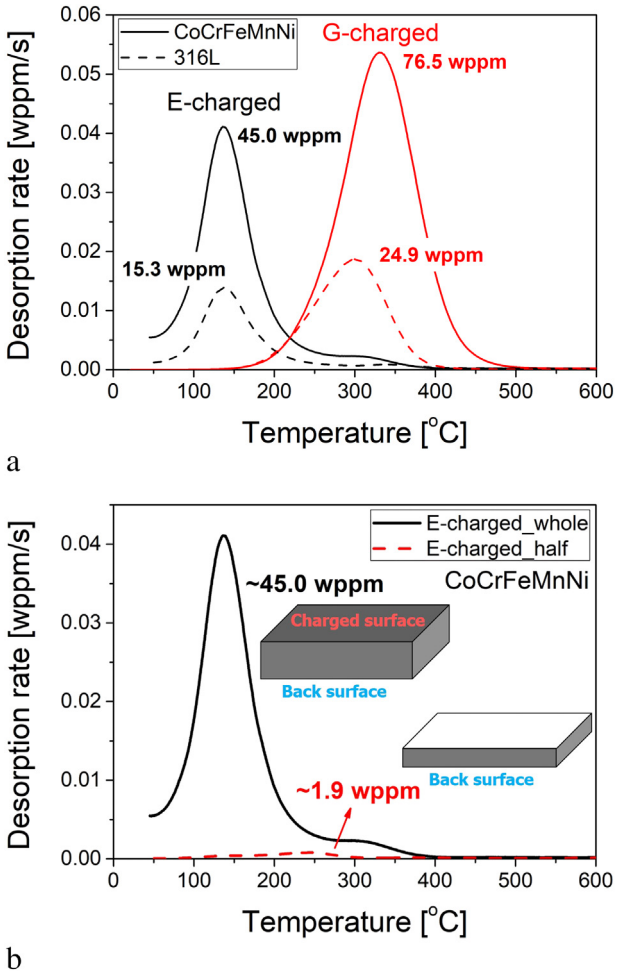

Fig. 2. TDS spectra of (a) HEA and 316L samples after either E-charging or G-charging and (b) a typical E-charged CoCrFeMnNi specimen and a half-piece specimen of which charged surface side was ground off right after E-charging.

in which C_0 is the local H concentration at the "surface" of an H-charged specimen, t_c is the charging time, and D_H is H diffusivity. According to the method used by Pontini and Hermida [33], C_0 can be determined as

$$C_0 = \frac{w \cdot C_M}{4}\sqrt{\frac{\pi}{D_H t_c}}, \quad (2)$$

where *w* is sample thickness (300 μm) and C_M is the mean H concentration in the sample (viz. ~45.0 wppm for CoCrFeMnNi and ~15.3 wppm for 316L). Assuming D_H for CoCrFeMnNi HEA to be similar to that of austenitic stainless steel such as 316L (~3.17×10^{-16} m^2/s at RT [19]), since (1) both have FCC structure, (2) the chemical constituents are similar [3], and (3) D_H of austenitic stainless steels is reported to be nearly-insensitive to the composition [19], C_0 are estimated to be ~1143 wppm for CoCrFeMnNi and ~419 wppm for 316L. These values, which are much higher than the mean H contents of both E- and G-charged samples, indicate that H indeed is highly concentrated near the E-charged surface.

The concentration profiles of H in both the samples, estimated using Eq. (1), are displayed in Fig. 3a. In the G-charged samples, H is homogeneously distributed through the thickness of the sample, which is expectable since the time (72 h)–temperature (300 °C) combination employed for charging allows for ample diffusion of H through the specimen [33]. The estimated H content profiles again prove that H atoms are highly concentrated near the surface (within the first several tens of microns from the surface as illustrated in Fig. 3a) for both E-charged HEA and 316L.

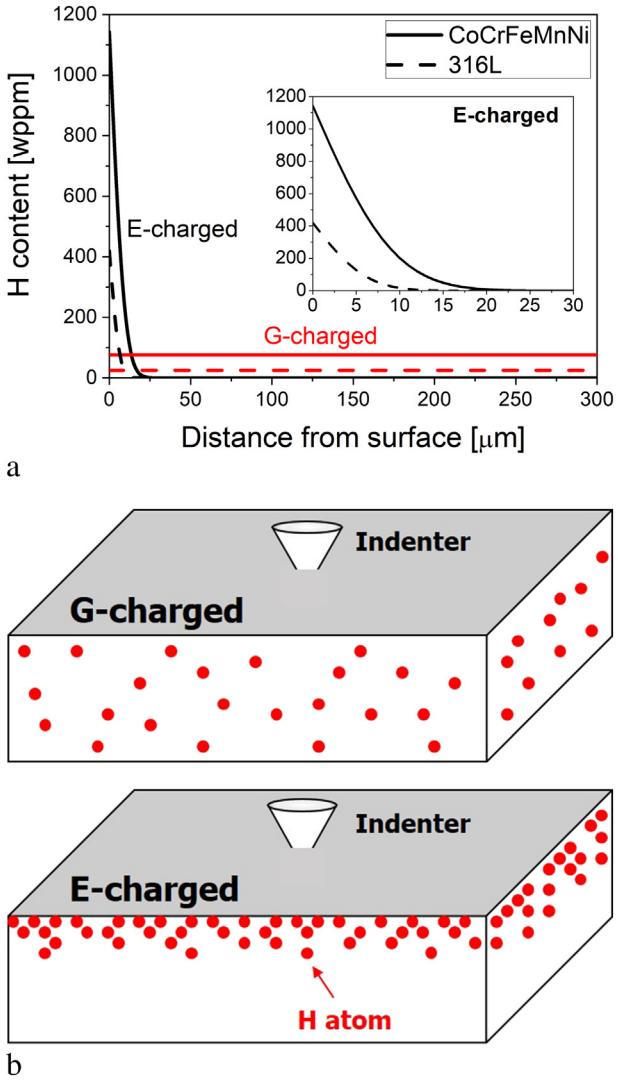

Fig. 3. (a) Estimated through-thickness distribution of H content in G- and E-charged HEA and 316L specimens (with the inset showing an enlarged view of the curves within 30 μm near surface), and (b) schematic illustrations of the H atoms distribution in the material underneath the indenter.

The above observations conclusively show that the E-charging process produces a steep gradient of H concentration near the surfaces of both CoCrFeMnNi HEA and 316L, whereas, and in contrast, G-charging process results in a homogeneous H distribution throughout the specimen. These differences in the H distribution, rather than any difference in the nature of the H trapping sites, are the reasons for the different temperature ranges observed for desorption peaks in Fig. 2a. Since microstructural analysis showed no evidence for the hydride formation in the hydrogenated HEA and 316L, H can reside only in the lattice and typical crystalline defects such as dislocations and grain boundaries [11,21,34].

The contrasting nanomechanical responses of E- and G-charged specimens are a direct consequence of the nature of H distribution in them. Since nanoindentation only probes the near-surface properties of a material, it is natural that a high C_0 near the E-charged specimen surface affects the measured properties in a marked manner, as illustrated in Fig. 3b. Similar to the case of conventional metals and alloys, this H-induced hardening in the HEA and 316L may be largely attributed to solid solution strengthening (SSS) [35] and H-enhanced slip planarity [11,36]. To examine the extent of SSS caused by H, additional nanoindentation experiments on CoCrFeMnNi samples that were E-charged to varying extents were performed. Results of these experiments, which are displayed in Fig. 4, show that hardness increases with both charging time and current density. Since the H content in the alloy can be expected to increase with either charging time or current density [37], it is reasonable to conclude that the observed hardness increments are indeed due to the increased H content in the alloys examined. Therefore, the local H contents in E-charged specimens (~1143 and ~419 wppm for CoCrFeMnNi and 316L, respectively) are high enough to induce obvious H-induced hardening, while those in G-charged samples (76.5 and 24.9 wppm for the HEA and 316L) are still below the threshold.

Additional supporting evidence for the inhomogeneous H distribution in E-charged sample and the H-content-dependent mechanical response is obtained from the fractographic analyses of charged and tensile tested samples reported by Zhao et al. [11] and Luo et al. [12]. Zhao et al. [11] observed dimples, which are indicative of ductile fracture, throughout the fracture surface in G-charged CoCrFeMnNi. Luo et al. [12], in contrast, found dimpled fracture morphology only in the inner regions but intergranular feature in the edges of cross-sectional sample after E-charging, which indicates H embrittlement near the charged surface due to a high H concentration.

Before closing, it is instructive to discuss the effects of H content on the H embrittlement in the CoCrFeMnNi HEA based on the above results. In our prior work [11,14], we reported no loss in plasticity upon G-charging CoCrFeMnNi HEA and the observation of ductile fracture features. While H-assisted intergranular fracture was reported in the same alloy in subsequent works [20,21], these studies pertain to very high H contents that are introduced under extremely severe conditions (≥100 MPa H_2 gas). Ichii et al. [20] pointed out that H embrittlement depends not only on the H-content but also on the strain-rate. Since the diffusivity of H in FCC alloys is very low, the H content may be the governing factor for H embrittlement in the alloys [31], which is in agreement with the E-charging tests and the nanoindentation results of the present study. When H content in the CoCrFeMnNi HEA (and probably all the FCC alloys) surpasses a certain threshold value, H-induced hardening occurs and so does H embrittlement (as evidenced by the plasticity loss indicated by the reduced h_f/h_{max} value), and both of them become severer with further increase in the H content. Nevertheless, there is no doubt that the CoCrFeMnNi HEA shows better resistance to H embrittlement than most FCC metals and alloys, including pure Ni and austenitic stainless steels, despite the much higher H solubility in it [11,12,21,23]; i.e. a higher threshold tolerating H's deleterious effects.

In summary, the influence of gaseous and electrochemical H charging on the nanomechanical behavior of the CoCrFeMnNi HEA and 316L were investigated through nanoindentation and TDS. The results show that E-charging enhances the hardness and reduces the ductility,

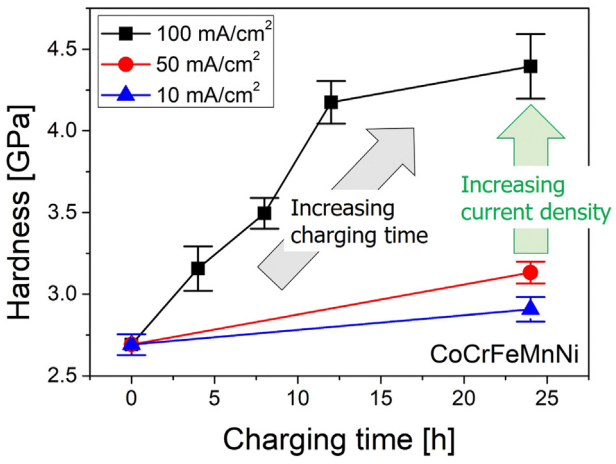

Fig. 4. Variation in nanoindentation hardness of the CoCrFeMnNi HEA that was E-charged under various conditions.

while G-charging does not cause noticeable changes in the properties despite the fact that it leads to higher total H content. Through TDS measurements and theoretical estimations, we show that the observed differences are due to the nature of charged H's distribution. Further investigations on H solubility and diffusivity, dissolved H's effects on the fracture toughness, in-situ slow strain-rate tests in H environments, fatigue and stress corrosion cracking behavior are essential for a comprehensive understanding of H embrittlement resistance of HEA in industrial scenarios.

YZ would like to thank the support from the Project funded by China Postdoctoral Science Foundation (No. 2017M620638). The work at Hanyang University was supported by the National Research Foundation of Korea (NRF) grants funded by the Ministry of Science, ICT and Future Planning (No. 2015R1A5A1037627 and No. 2017R1A2B4012255). JYS would like to thank the support from Korea Institute of Science and Technology (2E28060).

References

[1] B. Cantor, I.T.H. Chang, P. Knight, A.J.B. Vincent, Mater. Sci. Eng. A 375–377 (2004) 213–218.
[2] J.-W. Yeh, S.-K. Chen, S.-J. Lin, J.-Y. Gan, T.-S. Chin, T.-T. Shun, C.-H. Tsau, S.-Y. Chang, Adv. Eng. Mater. 6 (2004) 299–303.
[3] D.B. Miracle, O.N. Senkov, Acta Mater. 122 (2017) 448–511.
[4] I. Basu, V. Ocelík, J.Th.M. De Hosson, J. Mater. Res. 33 (2018) 3055–3076.
[5] B. Gludovatz, A. Hohenwarter, D. Catoor, E.H. Chang, E.P. George, R.O. Ritchie, Science 345 (2014) 1153–1158.
[6] J.C. Rao, H.Y. Diao, V. Ocelík, D. Vainchtein, C. Zhang, C. Kuo, Z. Tang, W. Guo, J.D. Poplawsky, Y. Zhou, P.K. Liaw, J.Th.M. De Hosson, Acta Mater. 131 (2017) 206–220.
[7] I. Basu, V. Ocelík, J.Th.M. De Hosson, Acta Mater. 157 (2018) 83–95.
[8] D.-H. Lee, M.-Y. Seok, Y. Zhao, I.-C. Choi, J. He, Z. Lu, J.-Y. Suh, U. Ramamurty, M. Kawasaki, T.G. Langdon, J.-I. Jang, Acta Mater. 109 (2016) 314–322.
[9] Y. Shi, L. Collins, R. Feng, C. Zhang, N. Balke, P.K. Liaw, B. Yang, Corros. Sci. 133 (2018) 120–131.
[10] H. Luo, Z. Li, A.M. Mingers, D. Raabe, Corros. Sci. 134 (2018) 131–139.
[11] Y. Zhao, D.-H. Lee, M.-Y. Seok, J.-A. Lee, M.P. Phaniraj, J.-Y. Suh, H.-Y. Ha, J.-Y. Kim, U. Ramamurty, J.-I. Jang, Scr. Mater. 135 (2017) 54–58.
[12] H. Luo, Z. Li, D. Raabe, Sci. Rep. 7 (2017) 9892.
[13] Z. Pu, Y. Chen, L.H. Dai, Mater. Sci. Eng. A 736 (2018) 156–166.
[14] Y. Zhao, D.-H. Lee, W.-J. Kim, M.-Y. Seok, J.-Y. Kim, H.N. Han, J.-Y. Suh, U. Ramamurty, J.-I. Jang, Mater. Sci. Eng. A 718 (2018) 43–47.
[15] G. Yang, Y. Zhao, D.-H. Lee, J.-M. Park, M.-Y. Seok, J.-Y. Suh, U. Ramamurty, J.-i. Jang, Scr. Mater. 161 (2019) 23–27.
[16] K. Verbeken, in: R.P. Gangloff, B.P. Somerday (Eds.), Gaseous Hydrogen Embrittlement of Materials in Energy Technologies, Woodhead Publishing, Cambridge 2012, pp. 31–33.
[17] A.-M. Brass, J. Chêne, Corros. Sci. 48 (2006) 3222–3242.
[18] Y. Zhao, M.-Y. Seok, I.-C. Choi, Y.-H. Lee, S.-J. Park, U. Ramamurty, J.-Y. Suh, J.-i. Jang, Scr. Mater. 107 (2015) 46–49.
[19] C. San Marchi, B.P. Somerday, S.L. Robinson, Int. J. Hydrog. Energy 32 (2007) 100–116.
[20] K. Ichii, M. Koyama, C.C. Tasan, K. Tsuzaki, Scr. Mater. 150 (2018) 74–77.
[21] K.E. Nygren, K.M. Bertsch, S. Wang, H. Bei, A. Nagao, I.M. Robertson, Curr. Opin. Solid State Mater. Sci. 22 (2018) 1–7.
[22] K.E. Nygren, S. Wang, K.M. Bertsch, H. Bei, A. Nagao, I.M. Robertson, Acta Mater. 157 (2018) 218–227.
[23] Y.J. Kwon, J.W. Won, S.H. Park, J.H. Lee, K.R. Lim, Y.S. Na, C.S. Lee, Mater. Sci. Eng. A 732 (2018) 105–111.
[24] Y. Zhao, D.-H. Lee, J.-A. Lee, W.-J. Kim, H.N. Han, U. Ramamurty, J.-Y. Suh, J.-i. Jang, Int. J. Hydrog. Energy 42 (2017) 12015–12021.
[25] H. Luo, Z. Li, W. Lu, D. Ponge, D. Raabe, Corros. Sci. 136 (2018) 403–408.
[26] B.N. Lucas, W.C. Oliver, Metall. Mater. Trans. A 30 (1999) 601–610.
[27] W.C. Oliver, G.M. Pharr, J. Mater. Res. 19 (2004) 3–20.
[28] Y.-T. Cheng, Z. Li, C.-M. Cheng, Philos. Mag. A 82 (2002) 1821–1829.
[29] F. Zhang, Y. Tong, K. Jin, H. Bei, W.J. Weber, A. Huq, A. Lanzirotti, M. Newville, D.C. Pagan, J.Y.P. Ko, Y. Zhang, Mater. Res. Lett. 6 (2018) 450–455.
[30] M. Dadfarnia, A. Nagao, S. Wang, M.L. Martin, B.P. Somerday, P. Sofronis, Int. J. Fract. 196 (2015) 223–243.
[31] S.P. Lynch, in: V.S. Raja, T. Shoji (Eds.), Stress Corrosion Cracking, Woodhead Publishing Ltd., Cambridge 2011, pp. 90–130.
[32] J. Crank, The Mathematics of Diffusion, Second ed. Oxford University Press, London, 1975.
[33] A.E. Pontini, J.D. Hermida, Scr. Mater. 37 (1997) 1831–1837.
[34] J.H. Ryu, Y.S. Chun, C.S. Lee, H.K.D.H. Bhadeshia, D.W. Suh, Acta Mater. 60 (2012) 4085–4092.
[35] A. Barnoush, M. Asgari, R. Johnsen, Scr. Mater. 66 (2012) 414–417.
[36] K.A. Nibur, D.F. Bahr, B.P. Somerday, Acta Mater. 54 (2006) 2677–2684.
[37] Y. Yao, X. Pang, K. Gao, Int. J. Hydrog. Energy 36 (2011) 5729–5738.